

Effect of Substrate Bias Voltage on Structure and Corrosion Resistance of AlCrN Coatings Prepared by Multi-Arc Ion Plating

Yihong Zhao^{1,*}, Yulong He¹, Qianyu Chen^{2,*}, Ziyu Gong¹, Zili Wang¹, Kai Wang¹,
Minjie Shi¹, Rongfa Chen¹

¹ School of Mechanical Engineering, Yangzhou University, Yangzhou, 225127, China.

² School of Engineering, University of Birmingham, Birmingham, B15 2TT, UK.

*E-mail: yihongzhao99@sina.com, QXC762@student.bham.ac.uk

Received: 19 May 2021 / Accepted: 5 July 2021 / Published: 10 August 2021

AlCrN coatings are deposited on 316L stainless steel by multi arc ion plating. The effects of different substrate bias voltages on the surface morphology, microstructure and corrosion resistance of AlCrN coating are studied. All the AlCrN coatings exhibit a face centered cubic structure with CrN as the main crystal phase. Moreover, the crystal growth direction has been changed by increasing the bias voltage, where the diffraction peak of (111) is decreased and the diffraction peak of (200) is increased. The surface morphologies show that the micro bumps on the coating surface are decreased, and the exfoliation pits are increased. The corrosion current of AlCrN coating is almost the same for the different bias voltages, but the peeling phenomenon of corrosion surface is reduced as the bias voltage increased.

Keywords: Corrosion resistance; AlCrN; Bias voltage; Multi-arc ion plating

1. INTRODUCTION

The 316L stainless steel has become one of the best candidate materials for the proton exchange membrane fuel cell (PEMFC) metal bipolar plate due to its preferable electrical and thermal conductivity, high mechanical strength, easy machining and low cost. However, in the anode environment of PEMFC, stainless steel is oxidized to form metal ions. These metal ions lead to catalyst poisoning through diffusion, and further diffuse to the proton exchange membrane, which causes ion exchange with the proton exchange membrane and pollutes the membrane electrode, thus affecting the performance of the battery [1]. In addition, in the proton exchange membrane fuel cell (PEMFC) cathode environment, the metal is easy to oxidize and produce a passive coating [2]. Although the

passive layer formed on the surface can protect the substrate to a certain extent, the conductivity of the passive coating is poor, which leads to the increase of the contact resistance between the bipolar plate and the gas diffusion layer and reduces the battery performance [3-4]. It is time-consuming to improve the corrosion resistance of stainless steel by adjusting alloying elements, and the coating modification of stainless steel has become popular in this field [5-9]. The coating method is easy to implement and has obvious protection effect. The combination of conductive and corrosion-resistant coating with stainless steel bipolar plate by different processes could improve the surface resistance of the bipolar plate while shielding corrosion ions, so as to improve the performance and lifespan of the entire PEMFC system [10-12]. The properties of coatings deposited under different process parameters are quite different, and it is extremely important to explore and optimize the parameters.

In this study, 316L stainless steel was used as the substrate, and the AlCrN modified layer was prepared on the surface by multi-arc ion plating technology. The AlCrN coatings were prepared by changing the bias voltage during deposition, and their microstructure and corrosion resistance were studied.

2. EXPERIMENT

2.1 Sample

In this study, 316L stainless steel with the dimension of $\Phi 40 \times 5$ mm was used as the substrate. The substrate surface was polished with 400, 600, 800, and 1000 mesh sandpapers, and then polished by using 1.5 μm diamond paste. Finally, ultrasonic cleaning was carried out in acetone and ethanol solution to remove oil and wax.

The AlCrN coatings were deposited by the PVD1050 multi-arc ion plating machine. The coating process was completed in a stainless steel vacuum chamber, and the background vacuum was better than 7×10^{-3} Pa. The coatings were deposited by an AlCr compound target ($\text{Al}/(\text{Cr} + \text{Al}) = 0.5$) in an Ar + N₂ atmosphere. A mass flow controller was used to control the flow rate of argon and nitrogen, and the substrate temperature was set to 450 °C. The substrate was bombarded and cleaned by Ar plasma for 20 min at a bias voltage of -220 V. After that, a Cr layer was prepared as the base layer on the surface of the sample, then a small amount of nitrogen was introduced for 2 minutes to deposit a CrN transition layer on the surface. Finally, increase the nitrogen flow to deposit the AlCrN coating for 1 hour. The bias voltages were set at -400, -500 and -600 V, and the target current was controlled at 150 A during the whole process.

2.2 Coating characterization

Field emission scanning electron microscope (FE-SEM, S-4800) and energy dispersive spectrometer (EDS) were used to characterize the surface and element composition of the coating. The phase of AlCrN coating was analyzed by X-ray diffraction (XRD, D8 Advance, Bruker, Germany) using a Cu K α radiation ($\lambda = 0.15406$ nm) operating at 30 mA and 40 kV. The incremental scanning

length was set to at 0.5° , and the 2θ range was between 30° to 65° with a scanning rate of $5^\circ/\text{min}$. The hardness of the coating was measured by a Vickers microhardness tester (HV-1000Z) at a load of 10 grams and a holding time of 10 seconds.

The potentiodynamic polarization of AlCrN coating and 316L stainless steel were tested by electro-chemical workstation (Chi660e) in 3.5 wt% NaCl solution at room temperature. The sample used as the working electrode has an effective exposure area of approximate 1 cm^2 . The platinum sheet was used as the counter electrode, and the saturated calomel electrode was used as the reference electrode. Before developing electro-chemical impedance spectroscopy, the open circuit potential was tested for 30 minutes. Finally, the potential polarization measurements were performed at a scan rate of 1.5 mV/s .

3. RESULTS AND DISCUSSION

3.1 Morphology observation

3.1.1 Surface topography and composition analysis

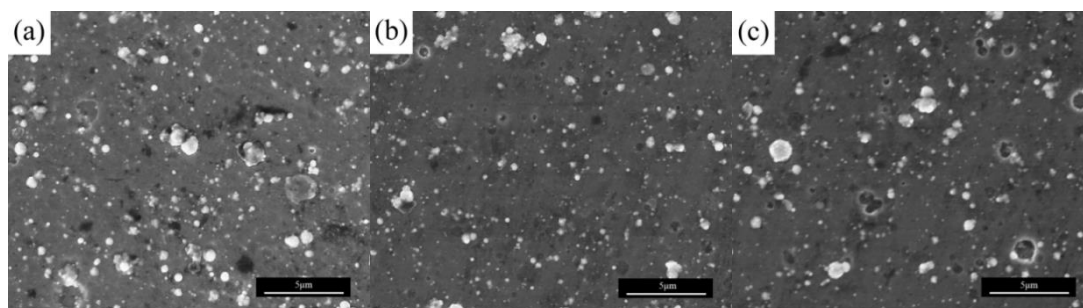


Figure 1. Surface FE-SEM morphologies of the AlCrN coatings, deposited at bias voltage of (a) -400 V ; (b) -500 V ; (c) -600 V

Figure 1 shows the surface morphologies of AlCrN coatings deposited under different bias voltages, and the results of the elemental composition are shown in Table 1. The coating surface is relatively flat and smooth. During the deposition process, the surface of the target produces a small molten pool due to the action of arc spots, which leads to violent evaporation of the target. Larger molten particles are sprayed and deposited on the surface of the substrate, forming droplets with a size of $1\text{-}2\text{ }\mu\text{m}$. When the bias voltage is -400 V , the number of large droplets on the surface of the coating is the greatest. As the bias voltage increases, the number of droplets on the coating surface decreases, and the surface tends to be flat. When the bias voltage increases to -600 V , the number of droplets on the coating surface decreases and more microcavities appear. With the increase of bias voltage, the ion bombardment is enhanced, leading to the sputter of the surface droplets [13]. When nitrogen initiates an expansion in the austenite crystal, it follows the anisotropy of the material. The phenomenon of concave dent can be observed as a result of surface deformation and the anisotropic lattice expansion in the nitrated layer [14]. When considering the arc ion plating process, the substrate with negative bias

voltage has a negative effect of repelling the negatively charged droplets. When the bias voltage increases, the repelling effect is enhanced and the number of droplets reaching the substrate surface decreases.

Table 1. Elemental composition analysis of AlCrN coatings deposited at different bias voltages

Bias/V	Al/%	Cr/%	N/%	Al/(Al+Cr)
-400 V	45.40	49.29	5.31	0.479
-500 V	46.81	47.28	5.91	0.497
-600 V	47.65	45.60	6.75	0.511

3.1.2 Cross-section morphology

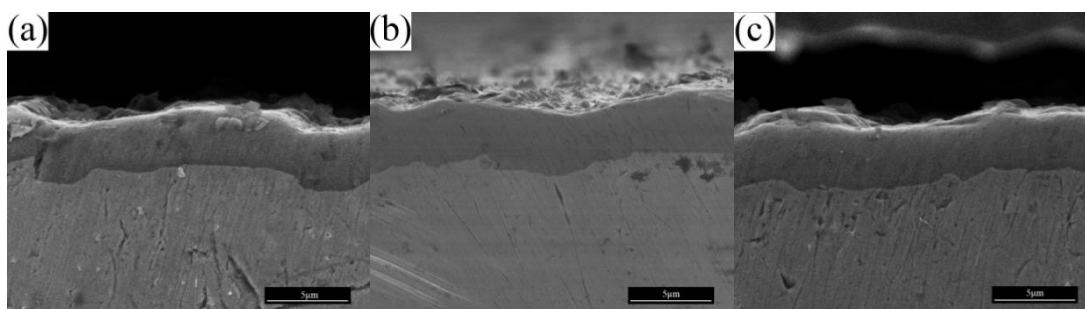


Figure 2. Cross-section FE-SEM images of the AlCrN coatings deposited at bias voltage of (a)-400 V, (b)-500 V, (c)-600 V

Figure 2 shows the cross-section morphology of the AlCrN coating. The parameters of hardness and thickness of the coating are shown in Table 2. The thickness of the coating shows a trend of firstly increasing and then decreasing, when increasing the substrate bias voltage. When a bias of -500 V is applied to the substrate, the thickness of the coating is the greatest, which is 2.5 μm . For other bias voltages, the thickness of the coating is between 2.3 μm and 2.4 μm . Figure 2 shows that the hardness of the coatings prepared under three kinds of bias voltages all firstly increases and then decreases when the load is 10 grams. When the bias voltage is -500 V, the coating has the greatest hardness of 2131 $\text{HV}_{0.01}$, and the hardness of other coatings is between 1915 and 2059 $\text{HV}_{0.01}$. The reason for the maximum hardness and thickness of the coating at -500 V is directly related to the magnitude of the bias voltage: driven by the bias electric field, the neutral atoms in the vacuum chamber are ionized and accelerated to reach the surface of the substrate, which promotes the coating-forming process and is conducive to the rapid growth of the coating; Cations (including Ar^+) bombard the growing coating under the electric field, which has the effect of sputtering on the coating, refining grain, forming the coating with more compact structure, and adjusting the crystal orientation and crystal structure in the coating. As the value of the negative bias voltage increases, both effects will increase [15]. When the bias voltage is greater than -500 V, the sputtering enhancement effect is greater than the adsorption enhancement effect. Therefore, when the bias voltage reaches -500 V, the AlCrN coating shows the

highest growth rate and is of the maximum thickness.

Table 2. Hardness and thickness of 316L and AlCrN coatings deposited on 316L

	316L	-400 V	-500 V	-600 V
Hardness/HV _{0.01}	183	1915	2131	2059
Thickness/ μm	--	2.3	2.5	2.38

3.2 Phase structure analysis

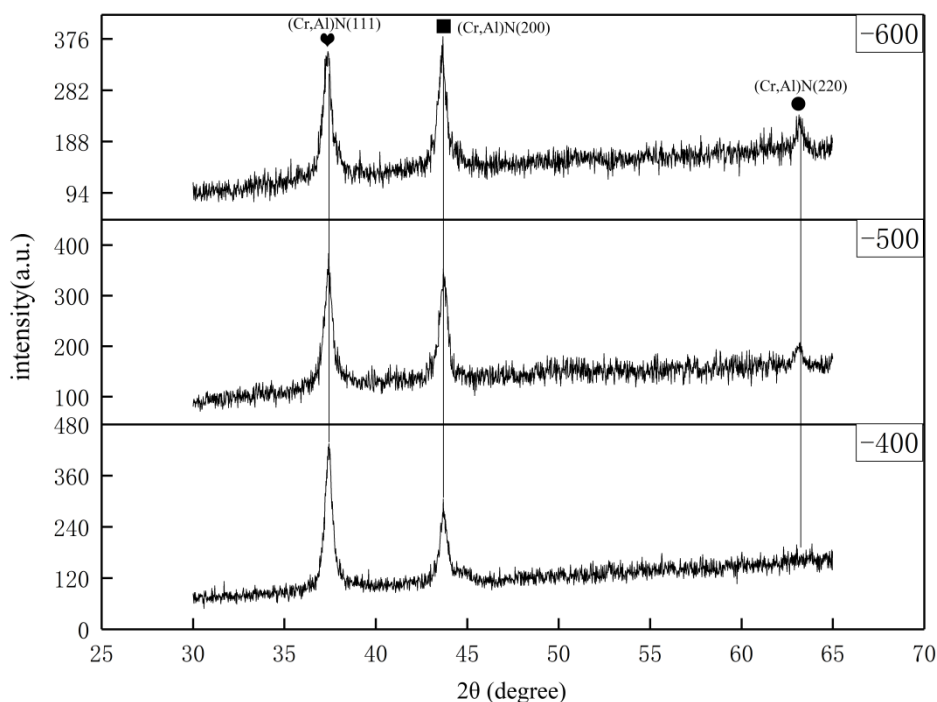


Figure 3. XRD patterns of the AlCrN coatings deposited under different bias voltages

Figure 3 shows the XRD patterns of 316L multi arc ion plating samples under different bias voltage. It can be seen from Figure 3 that the AlCrN coating shows a FCC structure, and there are (111) (200) and (220) oriented diffraction peaks between 30° - 65°. When the bias voltage is -400 V, the coating grows preferentially on (111) crystal plane. With the increase of bias voltage, the diffraction peak intensity of (111) crystal plane decreases gradually, and that of (200) crystal plane increases gradually. When the bias voltage is -500 V, the diffraction peak of (220) crystal plane appears, and it tends to increase with the increase of bias voltage. When the bias voltage is -600 V, the coating shows (200) preferred orientation. When the bias voltage increases, the ion energy and ion current density increase, the bombardment effect of high energy plasma on the deposited coating increases [16], and the ion diffusion ability increases. When the bias voltage increases, the plasma bombardment will lead

to the lattice distortion and the increase the internal stress of the coating. In order to release sufficient strain energy, the deposited ions diffuse to the (220) low potential energy surface. At the same time, with the increase of bias voltage, the FWHM of (111) crystal plane diffraction peak increases slightly, which indicates the grain refinement of the coating [17].

3.3 Corrosion behavior

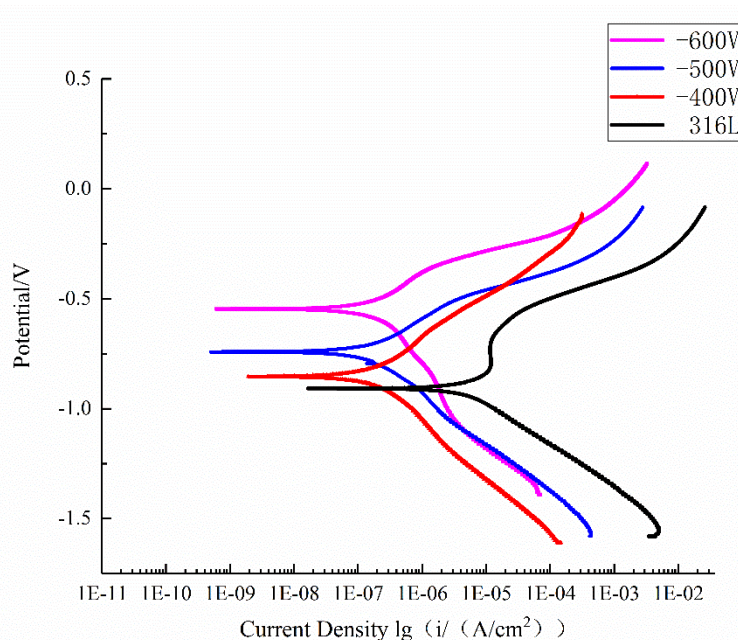


Figure 4. Potentiodynamic polarization curves of 316L and AlCrN coatings corroded in 3.5wt% NaCl solution. Scan rate: 1.5 mV/s

Figure 4 shows the potentiodynamic polarization curve of 316L stainless steel and AlCrN coated samples in 3.5wt% NaCl solution. The reference electrode is a saturated calomel electrode. It can be seen from Table 3 that the corrosion potential of the coated sample is increased and the corrosion current is reduced as comparing with 316L stainless steel. It indicates that the electrochemical corrosion performance of the coating is improved. The current density tends to be stable with the increase of the potential between -0.7 and -0.8 V, showing the characteristics of passivation. When the electrode potential continues to increase, this trend stopped and the current density increases. This electrode potential area is called a "pseudo passivation" area [18]. The short-term pseudo-passivation state can slow down the corrosion rate of the sample to a certain extent, but the protection state of the passivation film is easier to be broken and continue to be corroded [19]. In the simulated PEMFC working environment, whether it is the substrate or the sample after coating, the active dissolution zone of the potentiodynamic polarization curve of the sample after coating is large, but the activation-passivation zone almost disappears. The analysis indicates that the dissolved metal elements become ions and adhere to the surface of the catalyst to reduce its activity, the activation and dissolution zone is greater. As the substrate bias voltage increases, the corrosion current density of the

coating layer is not much different, and the corrosion potential increases compared to the substrate. When the bias voltage is -600 V, the AlCrN coating has the highest E_{corr} , which is -0.566 V, and I_{corr} is $0.11 \mu\text{A}/\text{cm}^2$. Therefore, the corrosion resistance is improved.

Table 3. Potentiodynamic polarization curve parameters of 316L and AlCrN coatings in NaCl solution

Sample	$I_{corr} / \mu\text{A} \cdot \text{cm}^{-2}$	E_{corr} / V
316L	9.31	-0.908
AlCrN coating (-400 V)	0.23	-0.863
AlCrN coating (-500 V)	0.14	-0.749
AlCrN coating (-600 V)	0.11	-0.566

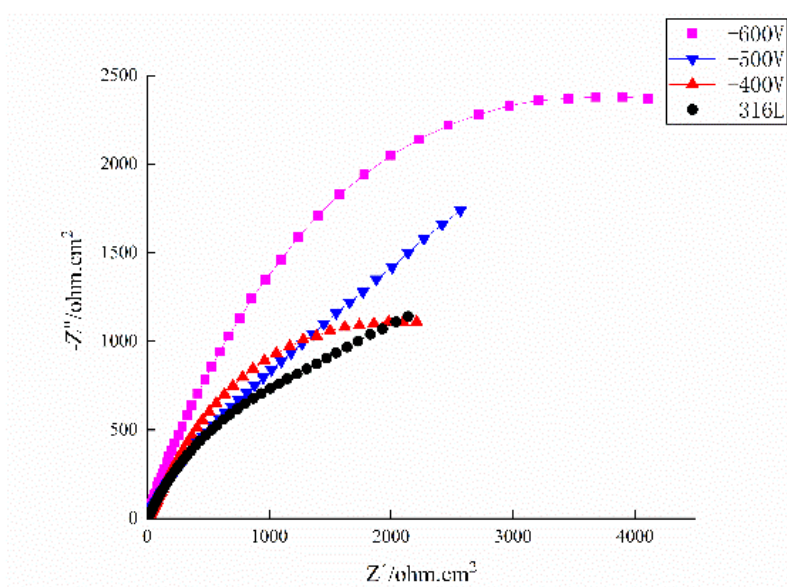


Figure 5. Nyquist plots of 316L and AlCrN coatings in NaCl solution

EIS test was carried out on the coated samples, and the corrosion circuit diagram of the coating was fitted according to the test results. Figure 5 shows the Nyquist curves of 316L coatings prepared at different bias voltages. It can be seen from Figure 5 that all impedance spectra have the same characteristics. In the high frequency region, each impedance arc consists of one single capacitive reactance arc. These semicircular arcs are not standard semicircles, but slightly flat. Since the diameter of the capacitive reactance arc is related to the charge transfer resistance of the electrode surface, the larger the capacitive reactance arc, the better the corrosion resistance of the material [20]. It can be seen from Figure 5 that the spectrum diameter is the largest when the bias voltage is -600 V, and the corrosion resistance of the coating is improved under this circumstance.

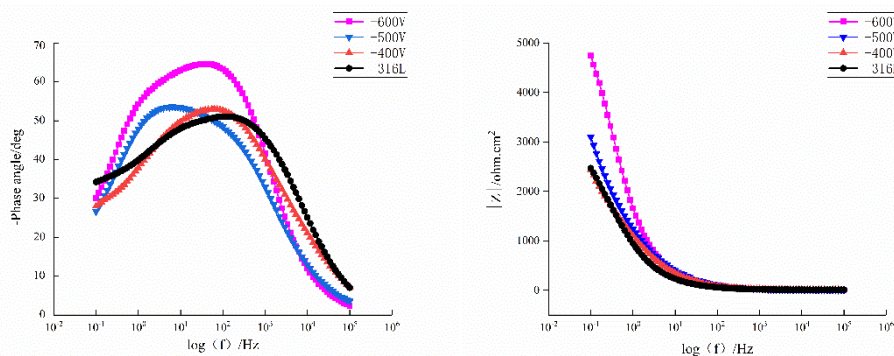


Figure 6. Bode plots of 316L and AlCrN coatings in NaCl solution

Figure 6 shows the bode curve of 316L stainless steel and coatings under different bias voltages. At a high frequency, the phase angle curve is close to 0°, and the impedance amplitude also tends to become a constant value, indicating that the electrolyte resistance is stable [21]. It can be seen from Figure 7 that when the bias voltage is -600 V, the coated sample shows the largest impedance modulus, the widest plateau and the largest phase angle (65°), indicating the structure is stable and the corrosion resistance of the sample is improved [22].

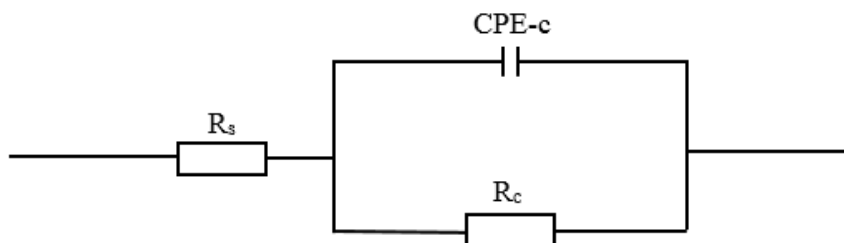


Figure 7. Equivalent circuit diagram of 316L and AlCrN coatings in NaCl solution

Figure 7 shows the electro-chemical corrosion equivalent circuit diagram of 316L stainless steel and AlCrN coating samples. Where R_s is the resistance of the corrosion solution, R_c is the coating resistance, and CPE-c is the coating capacitor.

Table 4. Fitting results of 316L and AlCrN coatings Electrochemical impedance spectra

Sample	$R_s / (\Omega \cdot \text{cm}^2)$	$R_c / (\Omega \cdot \text{cm}^2)$
316L	6.236	3.965×10^2
AlCrN coating (-400 V)	6.325	5.159×10^3
AlCrN coating (-500 V)	6.589	5.851×10^3
AlCrN coating (-600 V)	5.931	9.655×10^3

Table 4 shows the circuit fitting results. In the EIS spectrum under equilibrium potential, the value of R_c is proportional to the corrosion resistance of the material. It can be seen from Table 4 that the value of RC increases by an order of magnitude after the coating is deposited on the substrate surface. This is because in the critical state of pitting corrosion, the active anions will be adsorbed on the coating surface. The higher the charge transfer resistance is, the less anions will be on the metal surface. This will slow down the reaction speed of cathode and anode on the metal surface, as well as the corrosion rate. It indicates that the corrosion resistance of the material coated with hard coating has been significantly improved. The RC value of AlCrN coating under -600 V bias is the largest, which is also consistent with the polarization curve and EIS test results [23].

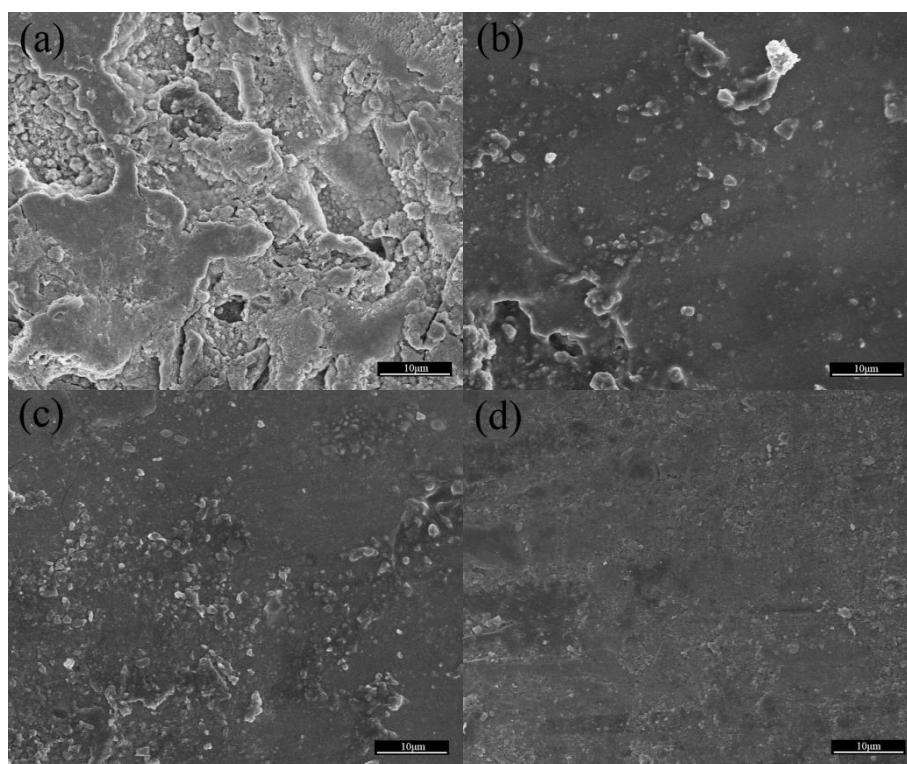


Figure 8. Corrosion morphology of (a) 316L and AlCrN coatings deposited under bias voltages of (b)-400V, (c)-500V and (d)-600V

Figure 8 shows the surface morphology of 316L SS stainless steel and its coating after polarization reaction. After corrosion, the surface of 316L SS substrate shows a large degree of spalling phenomenon. The obvious cracks and corrosion pits can also be identified. Due to the different corrosion rates along the different crystal directions, the size and the shape of corrosion pits are different. After the surface is modified with AlCrN, the corrosion spalling phenomenon is reduced, and the corrosion mechanism of the coating deposited under different bias voltages is different. With the increase of bias voltage, the depth of corrosion pits and cracks decrease. This is due to the formation of micropores and other defects in the coating during the deposition process, which will reduce the corrosion resistance of the coating. At the same time, when the AlCrN coating is chemically eroded, Cr

and Al can form a passive coating with good corrosion resistance on the surface of the coating to prevent the diffusion of corrosion medium into the substrate. The Cr and Al contents in the coating also have an influence on the corrosion resistance of the coating.

4. CONCLUSION

The AlCrN coatings deposited under different bias voltages have a FCC structure, and their surfaces are relatively flat and smooth. As the bias voltage increases, the preferred growth direction of the coating changes from (111) crystal orientation to (200) crystal orientation. The number of droplets on the surface decreases, and the hardness and thickness of the coating firstly increase and then decrease as the increase of bias voltage. The polarization curve of the sample after coating shows a higher corrosion potential and a lower corrosion current, indicating the improvement of the corrosion resistance of the sample. The corrosion current of the coating under different bias voltages is similar, but there are certain differences in the corrosion morphology. With the increase of the bias voltage, the surface of the sample tends to be flat, and the corrosion pits and cracks are very easy to be identified. At the same time, in the Nyquist diagram and the Bode curve, the capacitive arc with the greatest diameter and the highest phase angle for the sample deposited under -600 V bias voltage shows a better corrosion resistance.

References

1. H. Tawfik, Y. Hung and D. Mahajan, *J. Power Sources*, 163 (2) (2007) 755-767.
2. L.L. Zhang, G. Chen, R.X. Dai, X.H. Lv and D. Yang, S.J. Geng, *J. Power Sources*, 492 (2021) 229630.
3. Y. Wang and D.O. Northwood, *J. Power Sources*, 163 (1) 2007 500-508.
4. S.J. Lee, C.H. Huang and Y.P. Chen, *J. Mater. Process. Technol.*, 140 (1-3) (2003) 688-693.
5. J. Zhang and Q. Xue, S. Li, *Appl. Surf. Sci.*, 280 (2013) 626.
6. X. Zhang, X. Tian, Z. Zhao, J. Gao, Y. Zhou, P. Gao, Y. Guo and Z. Lv, *Surf. Coat. Technol.*, 364 (2019) 135.
7. B. Gao, X. Du, Y. Li, S. Wei, X. Zhu and Z. Song, *J. Alloys Compd.*, 797 (2019) 1.
8. S. Wan, H. Wang, Y. Xia, A. Tieu, B. Tran, H. Zhu, G. Zhang and Q. Zhu, *Wear*, 432-433 (2019) 202940.
9. S. Zhou, L. Wang and Q. Xue, *Surf. Coat. Technol.*, 206 (2011) 387.
10. C.K. Jin, K.H. Lee and C.G. Kang, *Int. J. Hydrogen Energy*, 40 (20) (2015) 6681-6688.
11. J.L. Cui, B. Jing, X. Xu, L.X. Wang, F.P. Cheng, S. Li, Z.S. Wen, S.J. Ji and J.C. Sun, *Int. J. Hydrogen Energy*, 42 (16) (2017) 11830-11837.
12. J. Jin, D.C. Zheng and H.J. Liu, *Int. J. Hydrogen Energy*, 42 (48) (2017) 28883-28897.
13. H. Zhao, X.H. Wang, Q.L. Liu, L.J. Chen and Z. Liu, *Trans. Nonferrous Met. Soc. China*, 20 (2) (2010) 679-682.
14. Z.Y. Gong, R.F. Chen, J. Li, P. Cao and H.R. Geng, *Int. J. Electrochem. Sci.*, 15 (2020) 1117-1127
15. L. Cunha, M. Andritschky, L. Rebouta, K and Pischow, *Surf. Coat. Technol.*, 116-119 (1999) 1152-1160.

16. F. Cai, M.H. Chen, M.X. Li and S.H. Zhang, *Ceram. Int.*, 43 (4) (2017) 3774-3783.
17. M. Sumadiyasa and I.B.S. Manuaba, *Buletin. Fisika.*, 19 (1) (2018) 28-34.
18. Z. Wang, Z. Feng, X.H. Fan and L Zhang, *Corros. Sci.*, 179 (2021) 109146
19. S.H. Zhang, Y.R. Li, Y.H. Wei, B.S. Liu, H.Y. Du, H. Wei and L.F. Hou, *Vacuum*, 185 (2021) 110042
20. Y.W. Cao, C.S. Guo, D.T. Wu and Y. Zou, *J. Alloys Compd.*, 867 (2021) 159126.
21. L. Li, Y.X. Chen, Y.J. Lu, S.J. Qin, G.H. Huang, T.T. Huang and J.X. Lin, *J. Mater. Res. Technol.*, 12 (2021) 904-915,
22. E. Boztepe, A.C. Alves, E. Ariza, L.A. Rocha, N. Cansever and F. Toptan, *Surf. Coat. Technol.*, 334 (2018) 116-123.
23. L. Cunha, M. Andritschky, L. Rebouta and K. Pischow, *Surf. Coat. Technol.*, 116-119 (1999) 1152-1160.

© 2021 The Authors. Published by ESG (www.electrochemsci.org). This article is an open access article distributed under the terms and conditions of the Creative Commons Attribution license (<http://creativecommons.org/licenses/by/4.0/>).